Imperial College London

Massachusetts Institute of Technology

MITei MIT Energy Initiative

<MSe²> A JOINT MIT-CNRS LABORATORY

Joule Effect in carbon/cement composites

Author:
Estelle Schurer

MIT Tutors:
Roland Pellenq
Thibaut Divoux
Nicolas Chanut

September 2019

Research internship
July 25^{th}- September 6^{th}

Acknowledgements

I would like to thank Roland Pellenq, Senior Research Scientist and Director of the Multi-scale Materials for Energy and Environment $(MSe)^2$, for giving me the opportunity to learn and participate in research in his laboratory. I truly enjoyed this 6 week internship and really hope I am able to come back for a longer period of time in the future. I would also like to thank my supervisors Thibaut Divoux, visiting researcher, and Nicolas Chanut, postdoctoral researcher, for their time and guidance as well as for giving me freedom and independence in my work. Finally, I would like to thank my colleagues Nancy Soliman (postdoctoral researcher) Traian Nirca, (visiting student) and Sama Taha (master student) for their collaboration and advice regarding methods, analysis and results.

Contents

1 Introduction

Concrete is one of the most widely used construction materials in the world [1]. It is composed of cement, water, sand and additional aggregates. The most widely used type of cement, Ordinary Portland Cement (OPC), has dominated concrete construction for the past 150 years with the production rate rising from 10 million tons in 1900 to 1500 million tons in 2000 [2]. However, concrete based structures are associated with deterioration along with resulting costs which could have been avoided by utilising a more durable material. Therefore, from an economic point of view, we need to find ways to make concrete more durable and more cost effective in terms of maintenance. In addition to this, the ongoing growth in the production of Portland cement as a result of world population increase represents a significant environmental impact. These include the energy required for its production and transportation, the emission of greenhouse gases during manufacture, the impact of mining, resource depletion and waste generation. Considerable energy and materials are also used during the rehabilitation of degraded structures [2]. Today, cement use in developing nations is expected to increase dramatically over the next 50 years. Additionally, with an increase in climate change associated with extreme weather conditions, the probability of infrastructure damage will also increase. This places heavy strains on the means of production and forces industry to re-evaluate its processes of manufacture in order to satisfy these demands [2]. Therefore, in a context of increasing durability and sustainability of concrete, the ongoing objective of the $(MSe)^2$ laboratory is to introduce new functionalities to concrete to lower its environmental footprint.

In this study, we used hardened cement paste compounds, essentially mixing cement powder and carbon black with water. These materials are very cheap, as cement powder costs approximately 0.1 USD/lbs and carbon black 6 USD/lbs, forming an economically viable composite material. Adding carbon black nanoparticles to cement paste introduces many new promising functionalities from which different applications arise. These include the synthesis of a conductive cement paste, as our studies show that for a given type of nanoparticles, there is a critical carbon concentration above which it forms a percolated network and shows conductive properties. The cement/carbon composite shows many other advantages such as hydrophobicity, energy storage, CO_2 capture and resistive heating, also known as the Joule Effect. The Joule effect is an increase in temperature which occurs as an electric current travels through a somewhat resistive material. This is what I decided to focus on during my 6 weeks internship.

As part of the $(MSe)^2$ team at the Massachusetts Institute of Technology (MIT), in collaboration with the French National Scientific Research Centre (CNRS) and the University of Aix-Marseille, I contributed to the overall understanding of the mechanical and electrical properties and microstructural arrangement of such carbon/cement composites.

1.1 Hardened cement paste

Ordinary Portland Cement (OPC) is composed of limestone/chalk and clay/shale. During the manufacturing process, it is heated to approximately 1500c to form clinker, the product of many complex reactions, containing essentially silicates and aluminates. It is then grinded into a powder to which 4% gypsum is added (Buenfeld, 2017). At this point, the cement is composed of many different phases. As the cement is mixed with water, it undergoes various hydration reactions, which form three main phases: calcium silicate hydrates (C-S-H gel), calcium hydroxide (Ca(OH)2, also known as portlandite) and ettringite. Despite the multiscale porous structure of CSH, it has a remarkable cohesion and acts as a binding agent in cement and concrete, therefore contributing to the materials mechanical properties during the hydration/hardening process (Ioannidou et al., 2016).
The hydration products have greater volume than the initial solids alone, hence the water filled space is gradually replaced by solids as the reaction takes place. The pores not filled by solid hydration products are called the capillary pores (mesopores). The principle hydration product, the C-S-H gel, also contains a significant volume of very small pores called gel pores (nanopores). In this sense, the pore system naturally divides into two pore populations; one becoming more numerous, and one becoming less numerous, as the reactions proceed (Jennings et al., 2008). Gel pores typically range from 1 to 2 nm, capillary pores from 2 to 100 nm. The capillary pores are interconnected to more than 92% [Figure 1.1].

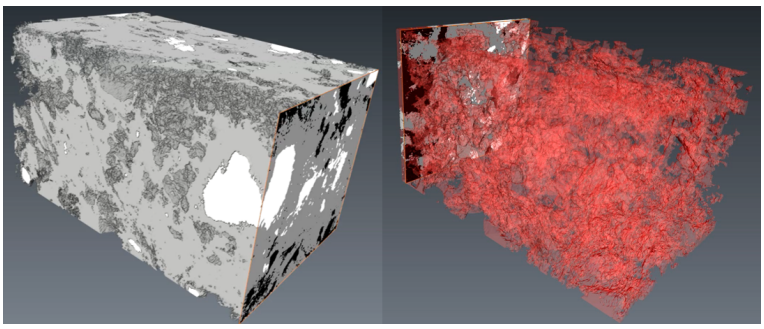

Figure 1.1: **X-Ray imaging of capillary porosity of cement paste. Left: white represents clinker, grey represents CSH. Right: red represents porosity (Pellenq, 2019)**

The quantities of the mix (water and cement) is determined by the water to cement ratio (w/c), which has a direct effect on the hydration process, hence the porosity and the mechanical properties of the material [Figure 1.2].

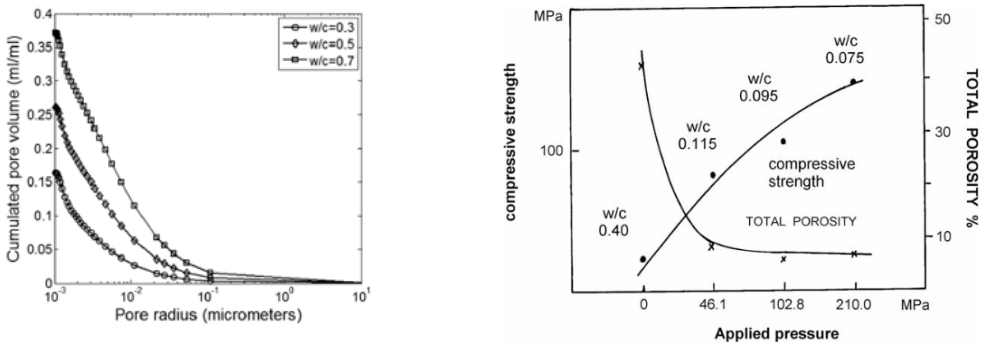

(a) (b)

Figure 1.2: **Effects of the w/c ratio on porosity and mechanical properties of cement** (a) Cumulative micropore size distribution of cement paste at 28 days for different w/c (Gong et al, 2014) (b) Dependence of compressive strength and total porosity (% weight) on applied pressure for different w/c ratios (Zivika, 2009)

Therefore, we use the important porosity of cement paste to incorporate carbon black nanoparticles and test the conductive and resistive properties of the produced samples.

1.2 From standard cement to heating cement: adding carbon nanoparticles

Carbon Black (CB) is a commercial form of black powder obtained by incomplete combustion of gaseous or liquid hydrocarbons. Carbon black typically contains more than 95% pure carbon as well as oxygen, hydrogen and nitrogen (Orion carbons, 2015). The fundamental building block of carbon black is the primary particle, 30 to 40 nm in size, but these almost never exist in isolation. They are strongly fused by covalent bonds into aggregates of size ranging from 85 to 500 nm [Figure 1.3]. Primary particles are somewhat conceptual, as they are no longer discrete and have no physical boundaries amongst them once the aggregate is formed. Once produced, individual aggregates join together in solution by Van der Waals forces to form larger agglomerates, which introduces a nanoscale porosity to the carbon black (ICBA, 2016). There are many types of carbon black, who differ according to their microstructure and porosity.

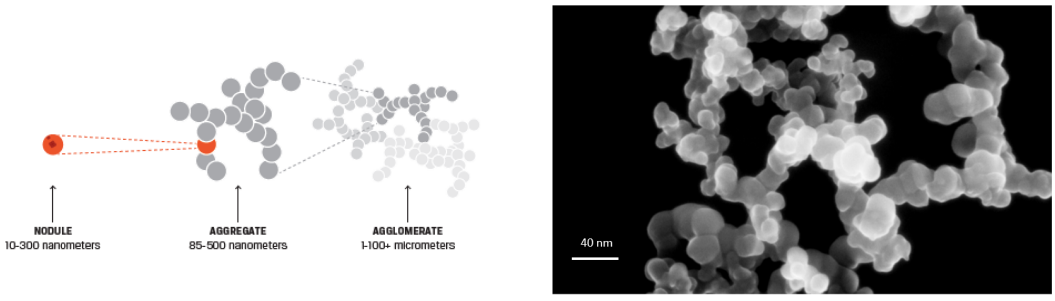

(a) (b)

Figure 1.3: **The microstructure of Carbon Black** (a) Sequence of Carbon Black structure development (ICBA, 2016). (b) Electron microscope view of Acetylene Black aggregate (Orion carbons, 2015)

In the $(MSe)^2$ laboratory, previous research on different cement/carbon samples showed that adding carbon nanoparticles (NP) to hardened cement paste increases its conductivity. We can see that beyond a certain threshold of approximately 2.5% carbon (of total weight) the carbon forms a percolated network and confers conductive properties to the cement. The conductive effect is found to be robust and obtained with different carbon nanoparticles such as Vulcan, Ketjen Black, PBX [Figure 1.4] (Pellenq, 2019).

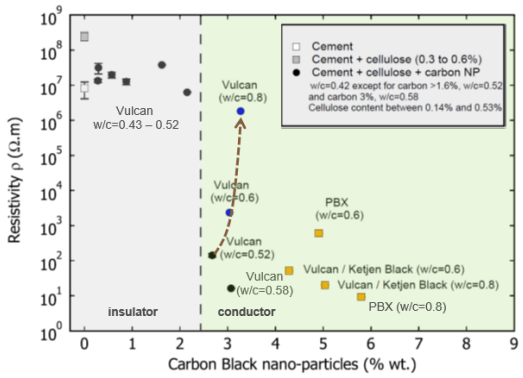

Figure 1.4: **Static conductivity measurements performed with flexible graphite foil contact -all samples dried at 60°C in an oven (Pellenq, 2019)**

In preliminary studies, two types of carbon were compared, PBX 55 (Cabot. Corp) and Acetylene Black (ABHC-01 by Soltex), for their well-known properties such as high charge acceptance and conductivity respectively. It was found that Acetylene Black was more effective in terms of the Joule Effect (Deman, 2019). Therefore, I decided to focus my work on the Acetylene Black resistance heating, more specifically on the role of the cement/carbon composites properties and composition. In my report I will also touch upon the effects applying the same measurements to mortar samples, which are composed of cement paste and added sand.

2 Experimental methods

2.1 Sample preparation

We have prepared cement/carbon samples with the following composition;

	w/c=0.42	w/c=0.6	w/c=0.8
Carbon % (of total weight) for Acetylene Black	0.88% 1.74% 2.59% 3.43%	1.11% 2.20% 3.26% 4.31% 5.33% 6.32%	1.32% 2.60% 3.85% 5.06%

Table 1: List of sample parameters to determine the influence of w/c ratio and carbon content on the properties of hardened cement paste

Firstly, the dry ingredients are blended together in a small beaker using a mechanical agitator with stirring blades [Figure 2.2 (a)]. Carbon black is more volatile than cement powder, making a perfectly homogeneous mix unobtainable. However, we continue mixing until it is as homogeneous as possible. Then, we add the water and place the beaker under the agitator again. Again, only an approximately homogeneous mix is obtainable, this time equally due to the hydrophobic properties of the carbon black.

(a) (b)

Figure 2.1: **Photos of tools and mix during sample synthesis** (a) Mechanical agitator used for mixing the different components of the cement/carbon composites (b) Final obtained mix once all components have been incorporated, ready to pour in the mould

The mixture is then poured in clear cylindrical moulds of 22 mm in diameter, which are sealed at each end using clear paraffin film. The samples are then placed in a saturated calcium oxide solution for seven days in order to control pH related to ion movement and avoid dehydration [Figure 2.2 (a)]. After seven days

they are taken out of the bath, and after 28 days the mechanical properties have evolved sufficiently for the samples to be unmoulded, in the same way this applies to standard cement samples. They are then cut into smaller samples of thickness ranging from 5 to 10 mm. For this we use a diamond blade fixed on a metallic saw. Finally, in order to insure good physical contact when measuring the current and temperature, we polish the samples on both flat surfaces with grinding paper of grit size 1000.

All samples are then drilled with holes of 1 mm in diameter and at a depth of 2 mm on opposite sides of the sample [Figure 2.2 (b)]. This will later allow us to insert probes for temperature measurements. The samples with w/c of 0.42 and 0.8 have relatively lower carbon percentages, as can be seen in Table 1. For the w/c=0.42 samples, this is due to the lack of workability that the addition of carbon induces on such an originally dry paste. In order to make such samples, we would have to use additives known as superplasticisers (polymers) to increase the flowability of the mixture. On the other hand, the high w/c=0.8 samples are weaker than other samples, which made them vulnerable to cracking and eventually breakage before or during the analysis.

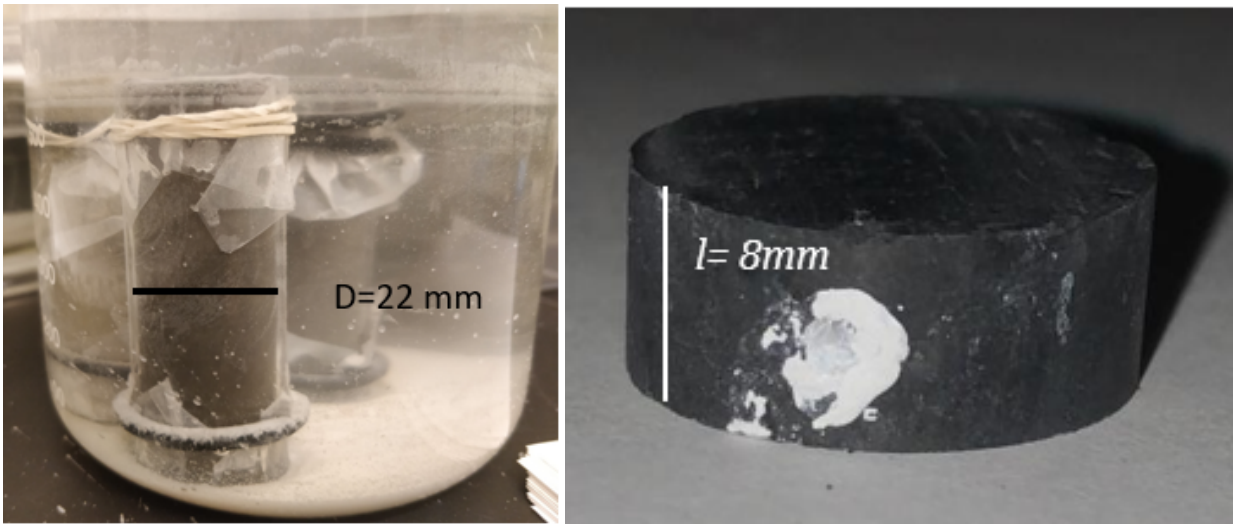

(a) (b)

Figure 2.2: **Photos of drying samples and finished sample** (a) Drying cement/carbon samples in (CaO) solution, in cylindrical moulds of 22mm diameter. (b) Sample of thickness 8mm, after unmoulding, cutting, polishing and drilling

2.2 Experimental setup: temperature increase measurements

As a certain voltage is applied, if the cement/carbon composite has a sufficient carbon percentage, its resistive nature causes it to heat up. We analysed this Joule Effect for voltages from 1 to 5 Volts.

To perform temperature evolution measurements, the sample is tightly clamped between two layers of conductive graphite paper, each connected to a terminal of

the same current generator (G) [Figure 2.3 (a)]. The temperature variations are measured using a double probe thermometer, from which the probes are inserted into the drilled holes. Additionally, we used thermal paste to fix the probes in place and ensure good thermal connection with the sample [Figure 2.3 (b)]. Additionally, we connected an ammeter to measure the corresponding current intensity (not pictured).

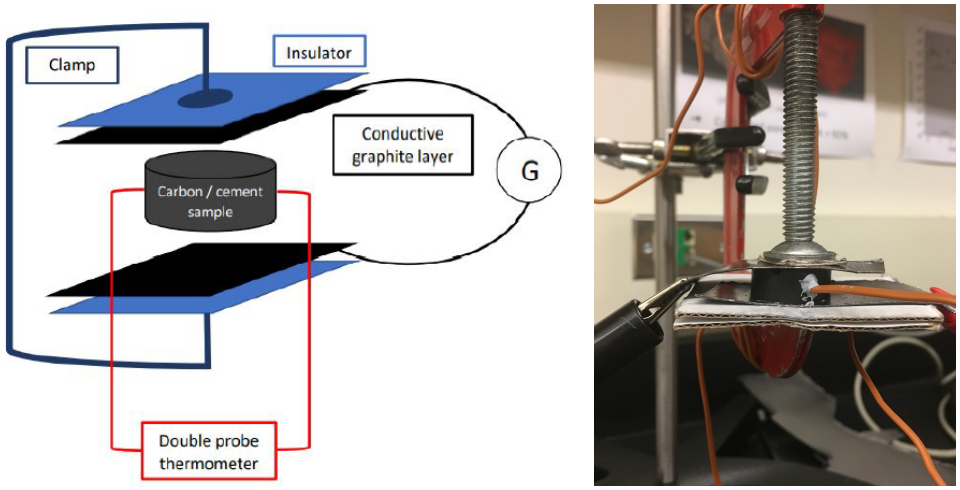

(a) (b)

Figure 2.3: **Experimental setup** (a) Diagram of the temperature measurement setup (Deman, 2019). (b) Photo of a cement/carbon composite being tested as a voltage is applied

For these cement/carbon samples, we used a temperature measurement interval of 2 seconds at each probe. The thermometer has a memory capacity of 499 measurements; therefore, each experiment takes around 16 minutes. The memory is then exported to the software FlukeView Forms (version 3.8) and treated in MATLAB.

All measurements were done at ambient temperature and pressure, with moisture content between 40% and 60%. We especially made sure that each sample was left to cool down between experiments, to ensure an initial state at room temperature.

3 Results and discussion: quantifying the Joule effect

3.1 Preliminary results

Firstly, the density ρ of each sample was measured from its mass M and volume V. As seen in Figure 3.1 below, these lie between 0.7 and 1.7 g/cm^3 and decrease with increasing w/c ratios. The densities also present a slow decay with carbon content but these variations are only marginal; from 1.66 to 1.75 g/cm^3, from 1.26 to 1.45 g/cm^3 and from 0.68 to 1.22 g/cm^3 for w/c of 0.42, 0.6 and 0.8 respectively.

We can therefore assume three fixed values of density for each w/c ratio, which are summarised in Figure 3.2.

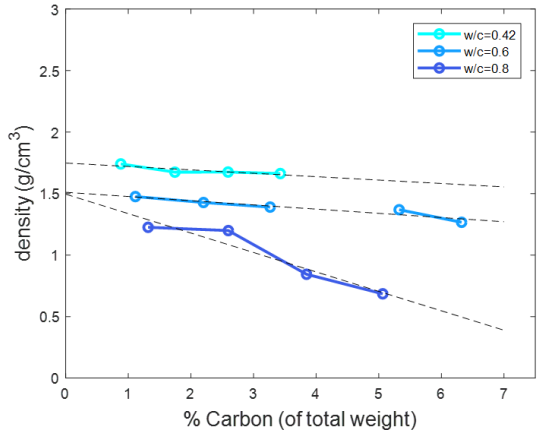

Figure 3.1: **Density of Acetylene Black carbon/cement samples with respect to carbon percentage at different w/c (ambient temperature and 40% relative humidity)**

	w/c= 0.42	w/c=0.6	w/c=0.8
Density ρ [g/cm^3]	1.69	1.39	0.99

Figure 3.2: **Average density of carbon/cement samples for each w/c ratio at ambient temperature and relative humidity of 40%**

3.2 Temperature rise analysis: model fitting

Upon measuring the temperature using the setup pictured in Figure 2.4, the following should be noted:
We applied a unit step function of voltage from 0 to U= 1,2,3,4,5V. As a result, the intensity I increases quickly from 0A to a value ranging from 0.05A to 1.7A, and once it reaches this value it remains constant. In fact, it increases so rapidly relative to the temperature (which takes on average 150 seconds) that we can assume it is constant throughout the duration of the experiment (taking the maximum value as that constant).
The temperature increases from T_0 (at t=0) within a time span which we will call the transient regime, towards a maximum value of T_∞. However, the temperature increases much more slowly than the intensity. The temperature eventually plateaus at the maximum value T_∞, indicating that it has reached the stationary regime. Below is a graphical representation of the behaviour of the temperature when a voltage of 4V is applied to a sample of w/c=0.42, 12% AB carbon.

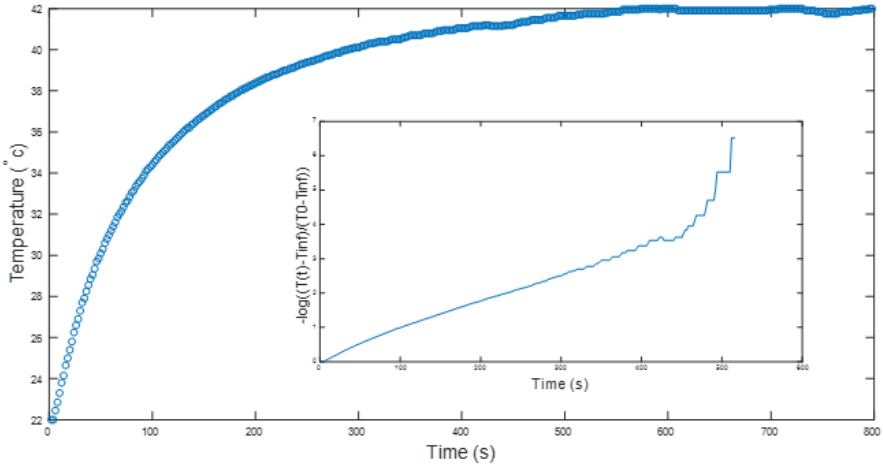

Figure 3.3: **Typical evolution of temperature T vs time t at voltage U=5V, for an Acetylene Black sample of w/c=0.42 and 12% carbon**

As seen in Figure 3.3, the temperature seems to follow a [1-exp(-x)] trend with time. Applying an energy balance to the experimental system, we were able to quantify this evolution. Firstly, we can assume the thermal energy arises as a result of a flux of heat by conduction, internal energy by Joule Effect and convection exchanges with the exterior at the surface of the sample, as follows;

$$\boxed{\text{Energy balance} : dU = dQ + dQ_{int} + dQ_{ext}} \tag{1}$$

Independently, we have

$$\begin{aligned} dU = \rho.C_m.V.dT = \rho.C_m.V\frac{\partial T}{\partial t}dt \\ dQ = [j_r(r)\cdot r - j_r(r+dr)\cdot(r+\delta r)]2\pi l.dt = \frac{\lambda}{r}\frac{\partial}{\partial r}(r\frac{\partial T}{\partial r})\delta r 2\pi r l.dt \\ dQ_{int} = \frac{j^2}{\sigma}V.dt = \frac{I^2 l}{\sigma S}dt \\ dQ_{ext} = hS(T_0 - T)dt \end{aligned}$$

where

C_m= specific heat capacity	$[J/K/Kg]$
$V = S \cdot l$= volume of sample	$[m^3]$
$j_r(r)$= heat current density(function of the sample radius)	$[J/m^2/s]$
S= exchange surface	$[m^2]$
λ= thermal conductivity of material	$[W/m/K]$
j=current density	$[A/m^2]$
σ= electrical conductivity	$[Sm^{-1}]$
I= current intensity	$[A]$
h= heat transfer coefficient $[W/m^2/K]$	

The energy balance (1) then becomes

$$\rho C_m V \frac{\partial T}{\partial t} = \frac{\lambda}{r}\frac{\partial}{\partial r}(r\frac{\partial T}{\partial r})\delta r 2\pi r l + \frac{I^2 l}{\sigma S} + hS(T_0 - T)$$

However, as the added carbon is evenly dispersed within the sample, its heating will be homogeneous. This allows all changes in temperature with respect to the radius of the sample to be neglected, which leaves;

$$\frac{\mathrm{d}T}{\mathrm{d}t} = \frac{hS}{\rho C_m V}(T_0 - T) + \frac{I^2}{\rho \sigma S^2 C_m}$$

Keeping the same units on either side of the equation and introducing $U = IR$ and $L = R\sigma S$;

$$\boxed{\frac{\mathrm{d}T}{\mathrm{d}t} = \frac{1}{\tau}(T_0 - T) + \frac{U^2\sigma}{\rho L^2 C_m}} \tag{2}$$

where

$$\boxed{\tau[s] = \frac{\rho C_m V}{hS}} \tag{3}$$

Solving equation (4) as the sum of a general and particular solution, applying the specified boundary conditions (T_0 for t=0 and T_∞ for t= ∞);

$$\boxed{T(t) = T_\infty + (T_0 - T_\infty)e^{-t/\tau}} \tag{4}$$

This corresponds to the evolution of the temperature of the sample with time and provides an appropriate fit to the collected data, with T_∞ and τ as free parameters. As seen in figure 3.6, we observe some "noise" towards larger times. This suggests that the fit could be improved by considering the variability of parameters. At large temperatures, parameters such as σ are most likely to be dependant on time t and temperature T, which in turn affects τ.

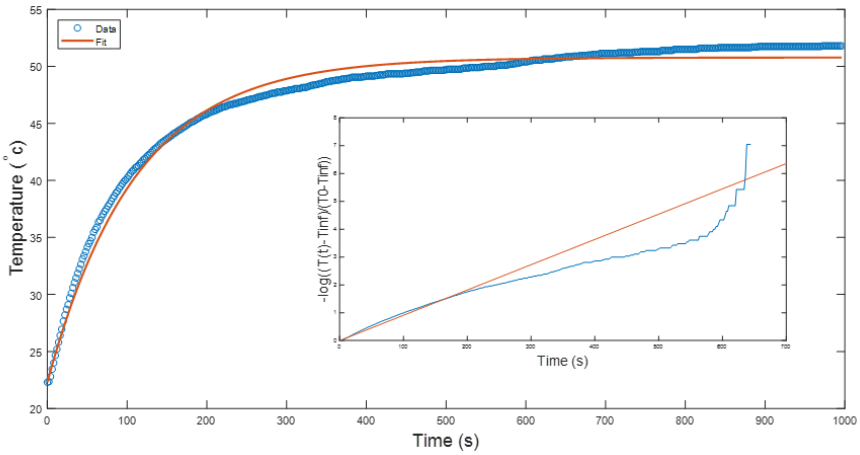

Figure 3.4

Figure 3.5: **Fitted curve of temperature T vs time t and estimate of parameter τ at voltage U=5V for an Acetylene Black sample of w/c=0.42 and 12% carbon**

An estimate of the values for τ and T_∞ can therefore be generated for each sample listed in the table in Figure 2.1. Figure 3.6 below displays the parameter τ (in seconds) of each sample, as well as the mean error associated with the accuracy of the fit (distance from the data to the fitted curve). We can see that τ is independent of the applied voltage, which is in agreement with equation (3) and contributes to the validation of the proposed model.

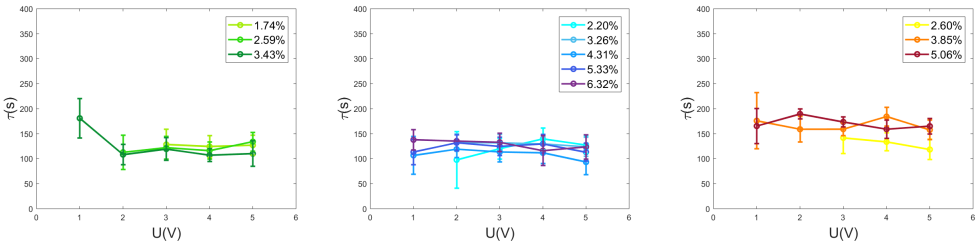

(a) (b) (c)

Figure 3.6: **Value of parameter τ (in seconds) with respect to voltage U for different Acetylene Black carbon content** (a) w/c=0.42 (b) w/c=0.6 (c) w/c=0.8

3.3 The effect of voltage

There are two regimes within the model; the transient regime, where the temperature increases rapidly, and the stationary regime where the temperature is constant and equal to T_{inf}. We can therefore set [equation (2)] $\frac{dT}{dt} = 0$ at stationary regime, $T = T_\infty$ and the net temperature difference $\Delta T = T_\infty - T_0$ to give;

$$\Delta T = \frac{\tau \sigma U^2}{\rho C_m L^2} \tag{5}$$

Assuming T_∞ is reached for each measurement, we can plot ΔT against U for all samples listed in Figure 2.1. For this, we are using empirical values of σ measured by another team member in previous experiments. These are representative of the "wet" electrical conductivity; at ambient temperature and humidity. As seen in Figure 3.7, ΔT is graphically proportional to U^2, which is in agreement with equation (5) and contributes to the validation of the proposed model.Additionally, we observe an increase of ΔT with carbon percentage, which is discussed further in section 3.5. However, there seems to be no evident differences in terms of w/c ratios.

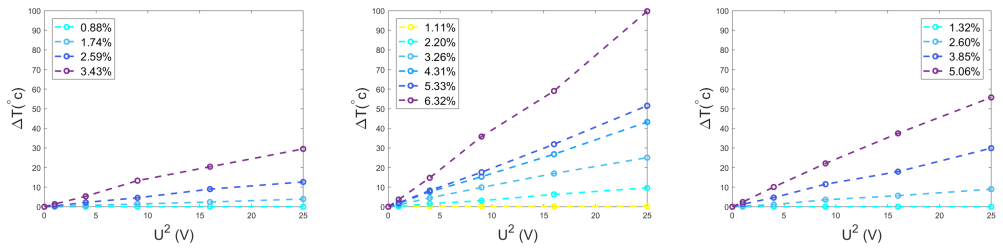

(a) (b) (c)

Figure 3.7: **Net temperature increase ΔT of Acetylene Black carbon/cement samples with respect to voltage squared U^2 and at different carbon percentage** (a) w/c=0.42, (b) 0.6 (c) 0.8

3.4 The effect of w/c ratio

As seen in Figure 3.8, the different w/c ratios do not seem to have a significant effect on net temperature difference ΔT for the Acetylene Black. The evolution of the curves, consistent with increasing voltage, seems to have a common trend for the different w/c ratios. Perhaps a slight divergence could be observed for samples with a higher carbon percentage, but further sampling would be required to support this.

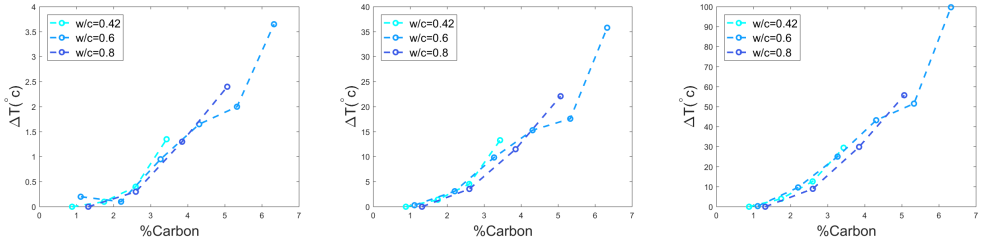

(a) (b) (c)

Figure 3.8: **Net temperature increase ΔT of Acetylene Black carbon/cement samples in terms of carbon percentage and at different w/c ratios** (a) U=1V. (b) 3V (c) 5V

3.5 The effect of carbon percentage

The carbon percentage is also an important factor; when it increases, ΔT increases accordingly. These results are reproducible for the different w/c, as seen in Fig 3.2 below. We can observe a percolation threshold marking the beginning of a significant temperature increase. When the conductivity of these samples were measured, it was observed that the percolation threshold increased with w/c ratio. As seen, our results for temperature increase are consistent with this deduction.

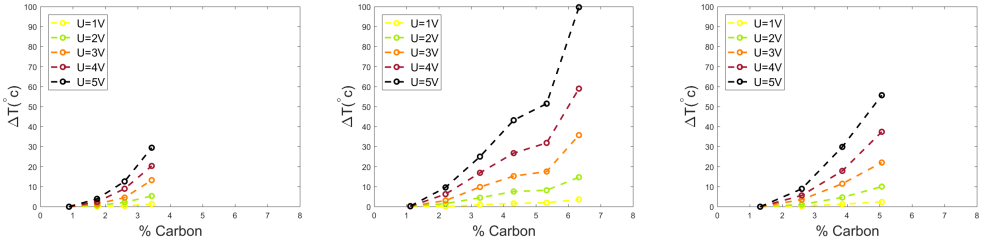

(a) (b) (c)

Figure 3.9: **Temperature increase with respect to carbon percentage, at different voltages** (a) w/c=0.42. (b) w/c=0.6. (c) w/c=0.8

3.6 Extraction of carbon/cement composite properties

Assuming the samples properties do not vary with time (an temperature), we can rearrange equation (5) to find the specific heat capacity C_m;

$$C_m[J/K/Kg] = \frac{\tau\sigma U^2}{\rho L^2 \Delta T} \tag{6}$$

Plotting the specific heat capacity for each w/c ratio gives us the following graph (Figure 3.5).

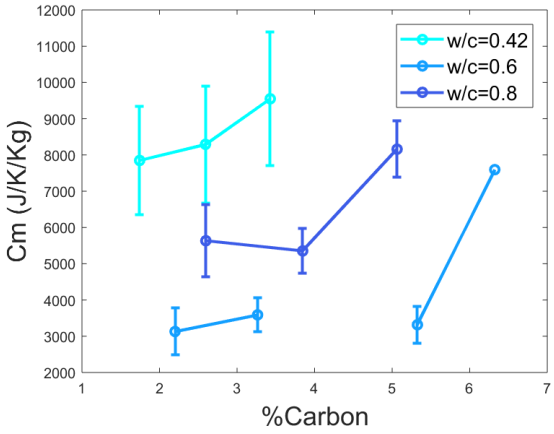

Figure 3.10: **Specific heat capacity (C_m) of samples with respect to carbon content in Acetylene Black at different w/c**

The values of C_m lie between 2000 and 9000 J/K/Kg, with higher values for w/c=0.42 and w/c=0.8 than for w/c=0.6. This would mean that they would need more energy to raise their temperatures by 1 Kelvin for 1 Kg of material. For reference, a table of specific heat capacities of standard materials is provided below. By comparison, the value for dry cement is somewhat different to the obtained measurements. It seems that adding carbon has contributed to increasing the specific heat capacity of the carbon/cement composites, especially for w/c ratios of 0.42 and 0.8. This can be observed on the graph whilst also considering the error bars.

	Steel	Glass	Aluminium	Cement, dry	Water
Specific heat capacity C_m [J/K/Kg]	468	792	887	1550	4187

Table 2: Specific heat capacities for base materials[14][15]

Knowing the expression for τ (5), we can rearrange for the coefficient of heat transfer, giving

$$h[W/m^2/K] = \frac{\rho C_m V}{\tau S} \tag{7}$$

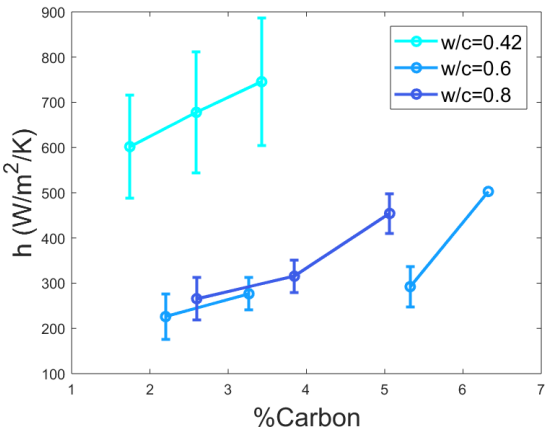

Figure 3.11: **Heat exchange coefficient (h) with respect to %C at different w/c**

The heat transfer coefficient in natural to forced convection in gases such as air range from approximately 10 to 200 W/m^2/K [16]. Here, the heat coefficient values that we find are larger.

3.7 Sample upscale: analysis of mortar

After analysing the previous carbon/ hardened cement paste samples, the same experiment was then conducted on a mortar at a larger scale. The objective of this test experiment is to consider the effect of adding sand to the carbon/cement sample, and to analyse the effect of upscaling. The test sample was prepared using the following properties.

	w/c	Carbon type	Carbon % (water wt)	Carbon % (total wt except sand)	Carbon % (total wt)
Mortar	0.8	AB	5%	2%	1.31%

Figure 3.12: **Table of quantities for the mortar synthesis**

The casting for the mortar sample was the same as for the cement samples, except for the cylindrical mold, which had a diameter of 50 ±1 mm and a height of 105 ± 1 mm. The sample was then left to harden in the calcium oxide solution, then in open air. After 28 days, the mortar was unmolded and polished to a grit size of 240. Because of the bigger surface area of the mortar, it was more difficult to obtain a flat, smooth surface. Consequently, the height of the sample decreased marginally during this process, leaving a sample of 81 ± 1 mm in height. The sample was then drilled on opposite sides (at the top and at the bottom, as seen in Figure 3.13) to allow us to insert the two probes. The same experimental setup as for the cement samples was used, using a clamp, graphite paper, thermal paste, a generator and a thermometer. Here, the clamp used was slightly bigger, as shown below in Figure 3.12.

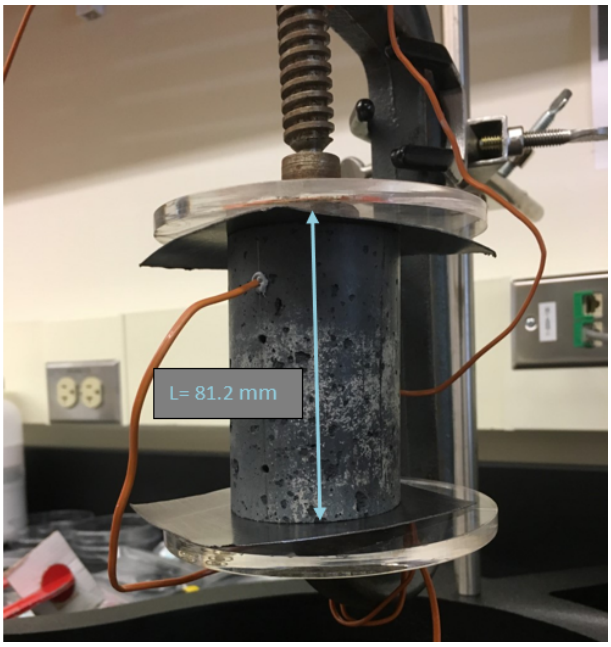

Figure 3.13: **Experimental setup for mortar temperature measurements**

The experiment was conducted similarly to the previous samples, but this time, after a process of trial and error, a voltage of 10 V was applied. The temperature increase was much slower than for the cement samples, therefore the time increment was set to 10 minutes instead of 2 seconds. The experiment was conducted for 3 hours and 30 minutes, to enable the sample to reach the stationary regime. In 3 hours and 30 minutes, I was able to observe the following temperature behaviours (Figure 3.13).

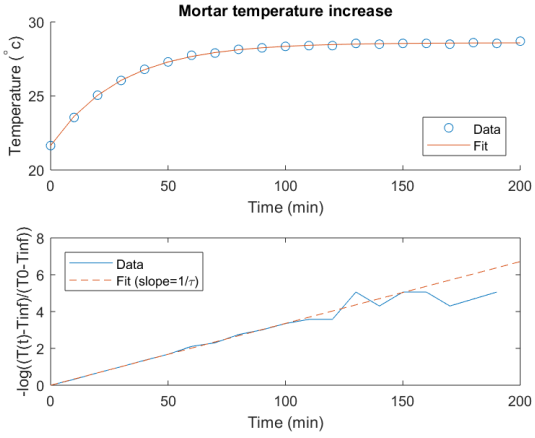

Figure 3.14: **Temporal evolution of temperature estimate of parameter tau for mortar sample of w/c=0.8 and 1.31% carbon content at U=10V**

Fitting the curve with the same proposed model, we are able to obtain an estimate of τ and T_∞. To extract the parameters, we need to first calculate the

electrical conductivity sigma of the material using the following;

$$R = UI$$
$$\sigma = \frac{l}{RS}$$

Computing σ and using equations (7) and (8) to find C_m and h, we obtain the values summarised in the table below (Figure 3.14).

	$\sigma[S/m]$	C_m [J/K/Kg]	h [W/m^2/K]
Parameter values	22.1	0.81	0.28

Table 3: Parameters based on fitted model, for mortar sample w/c=0.8 and 1.31% carbon content

4 Conclusion

After synthesizing and measuring various Acetylene Black carbon/hardened cement samples, we were able to define the effect of their composition on the Joule Effect. We saw that the temperature difference increases with the square of the applied voltage but was not significantly affected by w/c ratios. The joule Effect also increases with carbon content from a certain threshold, which agrees with previous analysis on the conductivity of these same samples. When fitting a model to the temperature increase, we observed that certain parameters such as the specific heat capacity and heat transfer coefficient had lower values for samples of w/c 0.6 only. Additionally, we saw that the proposed model also provided an adequate fit to larger mortar samples. By doubling the applied voltage we can observe a sufficient temperature increase, enabling us to compute the same material parameter values than for the cement samples.

We also found that less carbon could be added to low w/c samples due to decreased workability, and to high w/c samples due to decreased mechanical performance. I therefore made additional samples, with another member of the lab, containing Polycarboxylate Superplasticizer, which enabled us to have much more workable mixtures. Another member of the team, working on the conductivity of the carbon/cement composites, observed that superplasticizers do not have a negative effect and in fact increase their conductivity. When the influence of this superplasticizer on the Joule Effect is fully understood, it could potentially be used to increase the carbon percentage for lower w/c and therefore stronger cements, as well as more effective in terms of resistive heating.

References

[1] Taik, T.R. (2004) *Sustainability of the cement and concrete industries*. UWM Center for By-Products Utilization, University of Wisconsin-Milwaukee, Milwaukee, WI, USA

[2] Phair, J.W. (2006) *Green chemistry for sustainable cement production and use*. The Royal Society of Chemistry. Green Chem, 8, 763-780

[3] Buenfeld, N. (2017) *Materials CI1-132*. [Lecture notes]. Imperial College London, January.

[4] Deman, V. (2019) *Quantifying hydrophobicity and Joule effect in conductive carbon / cement paste composites*. [Report]. ENSTA, Paris

[5] Genoud, P. (2018) *Superconductive cements*. [3rd year research project report]. ESPCI, Paris.

[6] Gong et al., (2013) *Empirical estimation of pore size distribution in cement, mortar and concrete*. Journal of Materials in Civil Engineering. 26(7).

[7] International Carbon Black Association (2016) *Carbon Black Users Guide*.

[8] Ioannidou et al., (2016) *Mesoscale texture of cement hydrates*. Proceedings of the National Academy of Sciences of the United States of America. 113 (8), 20292034.

[9] Jennings et al., (2008) *Characterisation and Modelling of Pores and Surfaces in Cement paste: Correlations to Processing and Properties*. Journal of Advanced Concrete Technology. 6 (1), 5-29.

[10] Orion Engineered Carbons (2015) *What is carbon black*. Available from: https://pdfs.semanticscholar.org/1cda/47a9817ac09411d85c1b7c80546f26a9146f.pdf

[11] Pellenq, R. (2019) *Expanding Concrete Structural Elements Functionalities Urban Physics*. [Presentation]. MultiScale Material Science for Energy and Environment, MIT.

[12] Taylor, H.F. (1997) *Cement Chemistry*. London, Thomas Telford Publishing.

[13] Zivika, V. (2009) *Effects of the very low water/cement ratio*. Construction and Building Materials. 23, 3579-3582.

[14] Evans, P (2016) *Specific heat capacity of materials* The Engineering Mindset

[15] The Engineering Toolbox (2003) *Specific Heat of Solids*

[16] Engineers Edge (2019) *Convective heat transfer coefficients Table Chart*